ATOMIC-SCALE PROBE OF NOVEL PROXIMITY EFFECTS IN MANGANITE/CUPRATE THIN-FILM HETEROSTRUCTURES

Hao Zhang[1], Igor Fridman[1], Nicolas Gauquelin[2], Gianluigi Botton[2], John Y.T. Wei[1, 3]

[1]*Department of Physics, University of Toronto, Toronto M5S1A7, Canada*
[2]*Canadian Centre for Electron Microscopy, McMaster University, Hamilton L8S4M1, Canada*
[3]*Canadian Institute for Advanced Research, Toronto M5G1Z8, Canada*

ABSTRACT

Superconducting proximity effects that are anomalously long-ranged have recently been reported in manganite/cuprate thin-film heterostructures, and attributed to spin-triplet correlations involving odd-frequency pairing. To probe this novel scenario microscopically, we studied multilayer $La_{2/3}Ca_{1/3}MnO_3/YBa_2Cu_3O_{7-\delta}$ (LCMO/YBCO) thin films using scanning tunneling spectroscopy (STS), scanning transmission electron microscopy (STEM), x-ray diffraction and electrical transport. The STS measurements at 4.2 K observed no pairing gaps in the tunneling spectra on bilayer films down to 5 nm LCMO thickness. The atomic-scale STEM data revealed double CuO-chain intergrowths in the YBCO layer that form regions with the so-called 247 lattice structure. These nanoscale 247 regions do not show up in x-ray diffraction, but can physically account for the reduction in superconducting critical temperature (T_c) versus YBCO thickness. As further corroboration, we observed similar T_c reduction in $LaNiO_3$/YBCO multilayers, where $LaNiO_3$ is not ferromagnetic. These results suggest that microstructural defects, rather than magnetism, are responsible for the long-ranged attenuation of superconductivity reported in LCMO/YBCO heterostructures.

INTRODUCTION

In recent years, there have been numerous studies of the interplay between ferromagnetism and superconductivity in heteroepitaxial thin films comprising the ferromagnetic manganites and superconducting cuprates.[1-7] An observation of particular interest is the dependence of the superconducting critical temperature (T_c) on the *c*-axis layer thicknesses in $La_{2/3}Ca_{1/3}MnO_3/YBa_2Cu_3O_{7-\delta}$ (LCMO/YBCO) multilayers.[8,9] The length scale of this dependence has been attributed to extremely long-ranged superconducting proximity effect associated with spin-triplet pair formation.[6,10-20] Unlike spin-singlet pairs, spin-triplet pairs are not easily broken by an exchange field, and can thus penetrate deep into the ferromagnet. Theoretical models based on odd-frequency pairing have been proposed, to reconcile the spin-triplet pairing with *d*-wave orbital symmetry, which is known to predominate in YBCO.[21,22] Other interfacial mechanisms, such as charge transfer,[23-25] orbital reconstruction,[26] spin diffusion,[9] and induced magnetic modulation[27,28] are also believed to affect the superconductivity in LCMO/YBCO heterostructures.

Despite these prior studies, direct microscopic evidence for long-ranged proximity effect in LCMO/YBCO heterostructures has been lacking. In this paper, we report on an atomic-scale study of the phenomenon using scanning tunneling spectroscopy (STS) and scanning transmission electron microscopy (STEM), and correlate the results with macroscopic measurements including x-ray diffraction (XRD) and electrical transport. First, STS can be used to directly probe proximity effects in bilayer thin films by measuring the quasiparticle density of states (DOS) on the surface of the top layer.[29-31] A gap in the DOS spectrum would be a distinct signature of proximity-induced pair potential, and the gap-size dependence on layer thickness could provide a measure of the proximity length scale.[32] Furthermore, since STS is a local probe, it is inherently more sensitive than bulk resistivity measurements to spatial variations in the

quasiparticle DOS. Second, a crucial aspect of LCMO/YBCO heterostructures that has not been well studied is the microscopic stoichiometry of the YBCO layer. The Y-Ba-Cu-O compounds are exceptional among the cuprates in having CuO chains, the number of which per unit cell allows the cation stoichiometry to vary between the so-called YBCO-123 (single CuO chain), YBCO-124 (double CuO chain), and YBCO-247 phases (alternating single/double CuO chains) each with different optimal T_c.[33-39] Atomic lattices of the three phases of YBCO are shown in Figure 1. In thin-film heterostructures, microscopic variations in the YBCO stoichiometry could affect the resistively-measured T_c and thus the overall physical interpretation.

Our STS measurements at 4.2 K on bilayer LCMO/YBCO films observed no proximity-induced pairing gaps down to 5 nm LCMO thickness. Our STEM measurements in the bilayer films revealed YBCO-247 regions characterized by double CuO-chain intergrowths, which are largely absent in unilayer YBCO films. These nanoscale 247 regions do not show up in XRD, but can physically account for the reduced T_c measured in bilayer LCMO/YBCO films relative to unilayer YBCO films. Furthermore, we observed similar T_c reduction in $LaNiO_3$/YBCO heterostructures, where $LaNiO_3$ (LNO) is not ferromagnetic. These results suggest that microstructural defects, rather than magnetism, are responsible for the long-ranged attenuation of superconductivity reported in LCMO/YBCO heterostructures.

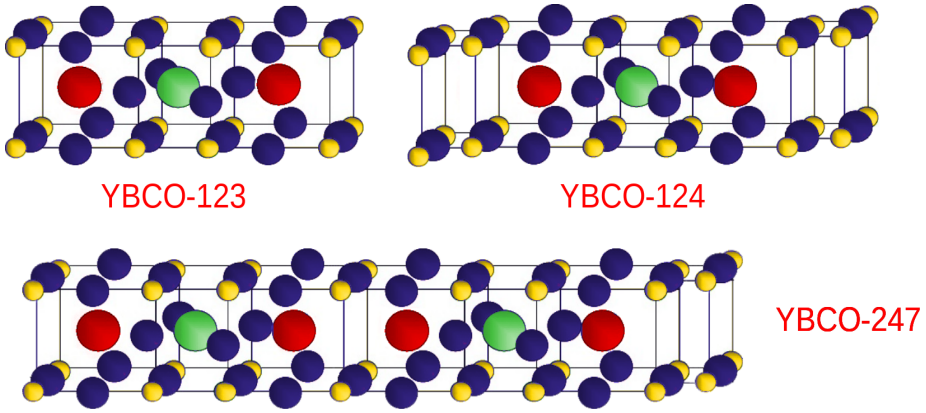

Figure 1: The lattice structures of YBCO-123, YBCO-124 and YBCO-247, with the Cu, Y, and Ba atoms color-labeled as yellow, green, and red, respectively.

EXPERIMENTAL

The LCMO/YBCO and LNO/YBCO multilayer films and the YBCO unilayer films used in our study were epitaxially grown on (001)-oriented (La, Sr)(Al, Ta)O_3 (LSAT) and $SrTiO_3$ (STO) substrates using pulsed laser-ablated deposition (PLD). Our PLD system is equipped with a 248nm KrF excimer laser (Coherent Compex 201) with a repetition rate of 2-5 Hz and fluence of ~ 2 J/cm^2, and the deposition was done at 700°-800°C in 200-500 mTorr of O_2. Following deposition, the films were annealed *in situ* by slow cooling from the growth temperature to 300°C in 45 minutes in 760 Torr of O_2 to fully oxygenate the YBCO layer. We grew various films ranging in LCMO thickness from 5 to 25 nm, YBCO thickness from 10 to 50 nm, and the LNO thickness was 25 nm. [40]

The STS measurements were made using a home-built scanning tunneling microscope (STM) with Pt-Ir tips in ~1 mTorr of ^{4}He exchange gas at 4.2 K. The typical junction impedance was ~10 GΩ. The conductance *dI/dV* spectra were obtained from numerically differentiating the average of 50 *I-V* curves at each tip location. The spectra were measured on several samples for each layer thickness, and at multiple locations on each sample to ensure reproducibility. [41]

The cross-sectional STEM images were taken using a FEI Titan 80–300 microscope fitted with a high-brightness field emission gun and CEOS aberration correctors for both condenser and objective lens aberrations. The microscope operated at 200 keV in scanning mode using the high-angle annular dark-field (HAADF) imaging method, which is sensitive to the atomic number contrast. The elemental identification made by the HAADF imaging was corroborated by atomic-scale electron energy loss spectroscopy (EELS). [42]

The XRD patterns were taken using θ - 2θ method with Cu K_a radiation from a Philips PW2273/20 X-ray tube. Finally, electrical resistance of the films was measured using standard ac lock-in technique in the four-contact configuration, in which silver contacts were sputtered onto the surface of the films in parallel strips. Temperature dependence of the resistance was recorded with a variable-temperature dipper probe inside a liquid helium dewar, and the sample temperature was monitored with a Cernox sensor to 0.1 K accuracy.

RESULTS AND DISCUSSION

The STS data taken on bilayer LCMO/YBCO films grown on STO substrates are shown in Figure 2. Figure 2a) shows the *dI/dV* spectra for three films, ranging from 10 nm to 20 nm of LCMO deposited over 20 nm of YBCO. These plotted spectra have been normalized by their values at 50 mV. These spectra have a characteristic V shape with some asymmetry, and substantial conductance at zero bias, indicating finite DOS at the Fermi level. No clear gap structure is seen, in contrast to the spectrum taken on a unilayer YBCO film as shown in Figure 2b). The bilayer spectra data are also qualitatively similar to data taken on a unilayer LCMO film as shown in Figure 2c). Similar V-shaped spectra have been seen in other transition-metal

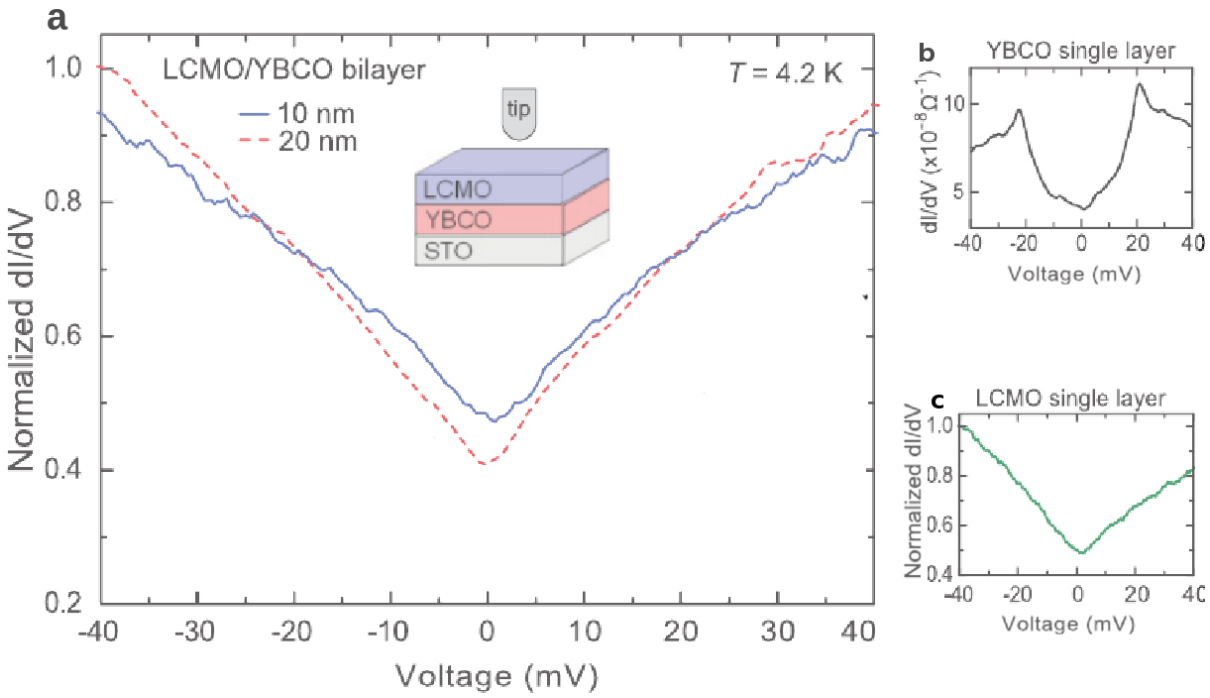

Figure 2: a) Normalized conductance spectra measured by STM at 4.2 K on LCMO/YBCO bilayers, for 10-nm-thick (blue solid curve) and 20-nm thick (red dashed curve) LCMO, respectively. These spectra on the bilayer films are distinct from those measured on a unilayer YBCO film grown under similar condition shown in panel b), but is similar to those measured on a unilayer LCMO film shown in panel c).

oxides, and appear to be characteristic of strongly-correlated oxide materials.[3, 43] When the LCMO layer is reduced to 5 nm, the *dI/dV* spectra (not shown) also look V-shaped similar to unilayer LCMO films. Thus down to 5 nm of LCMO thickness, there is no clear signature of superconducting proximity effect in bilayer LCMO/YBCO bilayer. These observations are consistent with conventional short-ranged proximity effect associated with strong suppression of spin-singlet pairing in the half-metallic LCMO layer. [41]

Figure 3 shows a high-resolution HAADF STEM images taken near the LCMO/YBCO interface, over the cross section of a 25 nm/50 nm bilayer LCMO/YBCO film grown on LSAT substrate. The color labels indicate different elements as identified from the HAADF STEM images, with the Cu, Y, and Ba atoms color-labeled as yellow, green, and red, respectively. To the right of the LCMO/YBCO interface, there are three defect-free unit cells of YBCO-123 characterized by single CuO chains between Ba atoms, followed by a unit cell of YBCO-124 characterized by double CuO chains between Ba atoms. This alternation of single and double CuO chains forms a unit-cell of YBCO-247, which is effectively a superlattice of YBCO-123 and YBCO-124 building blocks. Further on the right of Fig. 2a) is another YBCO-247 unit cell, also containing both a single and a double CuO chain. Between the two YBCO-247 unit cells, a unit cell of YBCO with missing CuO chain is seen, in which two adjacent Ba layers join together with no CuO chain in between. Such chain-less region can be explained in terms of compensation to the double CuO chains in the YBCO-247 regions, as the YBCO target used for PLD has 123 stoichiometry.

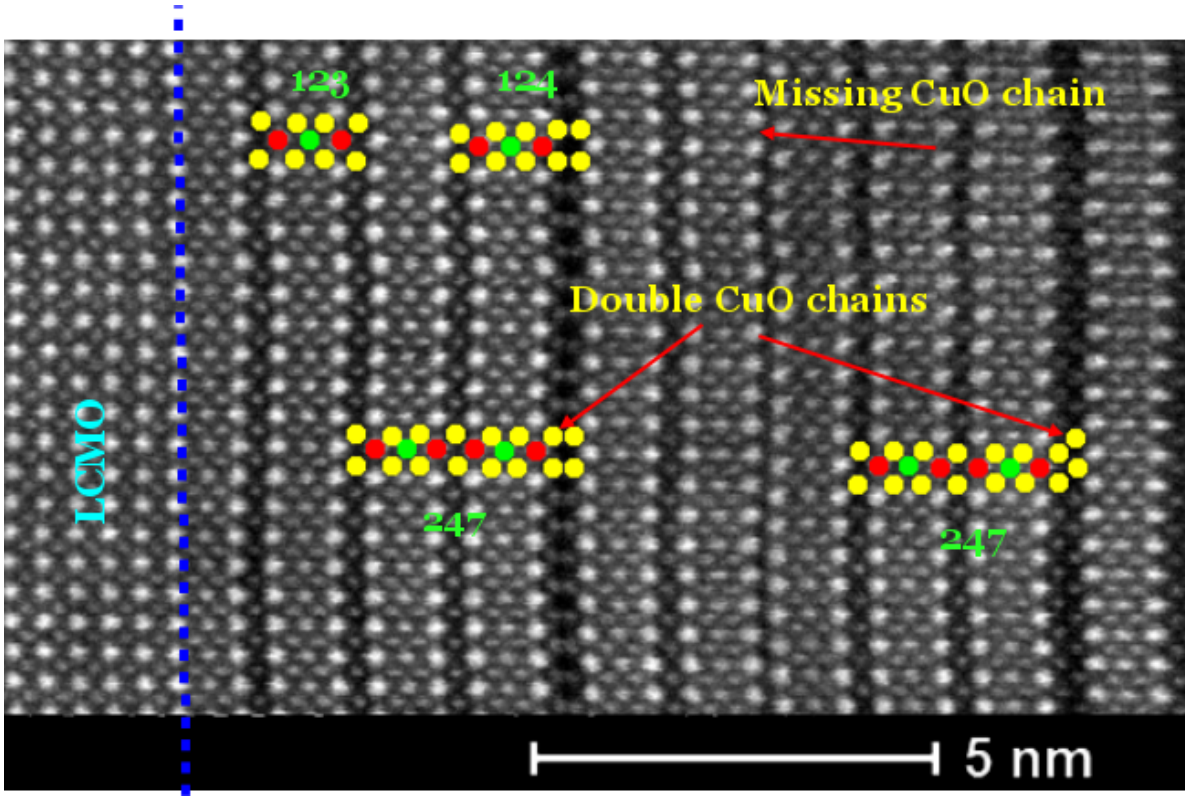

Figure 3: High-resolution HAADF-STEM images of a 25 nm/50 nm bilayer LCMO/YBCO film grown on (001)-oriented LSAT substrate, taken near the LCMO/YBCO interface. Intergrowths of double CuO chains which form nanoscale 247 regions can be seen. The Cu, Y, and Ba atoms are color-labeled as yellow, green, and red, respectively.

To examine the pervasiveness of the nanoscale YBCO-247 intergrowths, we compare the STEM images of a bilayer LCMO/YBCO versus a unilayer YBCO. In the bilayer LCMO/YBCO film shown in Figure 4a), nanoscale YBCO-247 regions appear throughout the YBCO layer, with double CuO chains indicated by the arrows. On the other hand, in the unilayer YBCO film grown under similar conditions as shown in Figure 4b), the double-chain intergrowths are mostly absent. Interestingly, the nanoscale YBCO-247 regions in the bilayer LCMO/YBCO film seen in the high-resolution STEM image do not appear in XRD. As shown in Figures 4c and 4d, the locations of the XRD peaks of a bilayer LCMO/YBCO film and a unilayer YBCO film are indistinguishable. All the major peaks are identified in terms of the *c*-axis lattice of either YBCO-123, LCMO or LSAT, although the peaks for LCMO and LSAT are not distinguishable because of their close lattice parameters. By relating the YBCO (005)-and (007)-peaks with $2\theta = 38.55^{\circ}$C and $2\theta = 55.06^{\circ}$C in the bilayer XRD, respectively, we find the *c*-axis lattice parameter of the YBCO layer in our bilayer film to be 11.68 Å, in agreement with fully oxygenated YBCO-123.[44] It should be emphasized that no peaks associated with YBCO-247 are visible in the XRD patterns of both bilayer and unilayer films, within the resolution of our instrument.

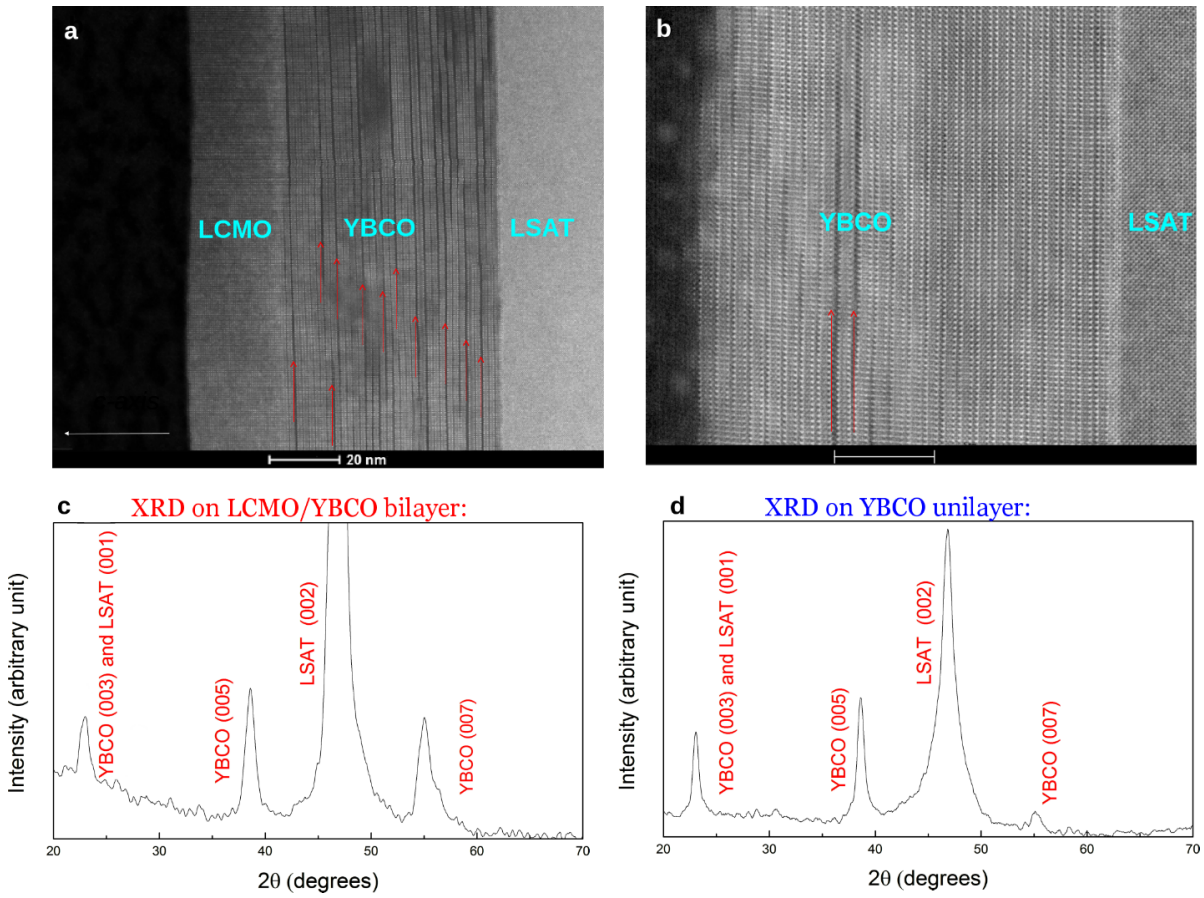

Figure 4: Comparison of the double-CuO chain intergrowths in bilayer LCMO/YBCO and unilayer YBCO films. Panel a) shows an STEM image of a bilayer LCMO/YBCO film. YBCO-247 regions appear throughout the YBCO layer, as shown by arrows indicating double CuO chains. On the other hand, the double-chain intergrowths are largely absent in unilayer YBCO film, as shown in panel b). The XRD peak locations for a bilayer LCMO/YBCO film, shown in panel c), and for a unilayer YBCO film, shown in panel d), are indistinguishable. The nanoscale YBCO-247 regions that appear in the bilayer film STEM images do not show up in the XRD pattern, within the resolution of our instrument.

The resistively-measured T_c in our bilayer LCMO/YBCO thin films can be affected by the presence of nanoscale YBCO-247 regions. Figure 5 plots the resistance R vs. temperature T data taken on various films. Each R vs. T curve is normalized to its R value at room temperature to facilitate comparison. The unilayer YBCO films grown on LSAT or STO substrates show sharp superconducting transitions with T_c near 90 K, consistent with fully-oxygenated YBCO-123. These results indicate that the resistive T_c of the YBCO layer is largely insensitive to the lattice mismatch with the substrate material, down to 25 nm YBCO thickness at least. However, the 25nm/25nm bilayer LCMO/YBCO film shows a much lower and broader T_c, near 60 K, than any of the unilayer YBCO films, indicating that the addition of an epitaxial LCMO overlayer significantly reduces the resistive T_c in the YBCO layer. We can plausibly attribute this T_c reduction to the nanoscale YBCO-247 regions seen in our high-resolution STEM images, since YBCO-247 has generally shown lower T_c than either YBCO-124 or fully-oxygenated YBCO-123 according to bulk studies.[45,46] We note that an alternative explanation of this T_c reduction in terms of under-oxygenated YBCO-123 is not likely, since the LCMO overlayer was grown *in situ* at an even higher oxygen pressure than the YBCO layer, and the entire bilayer was given sufficient time to fully oxygenate during *in situ* post-annealing in 760 Torr of oxygen.

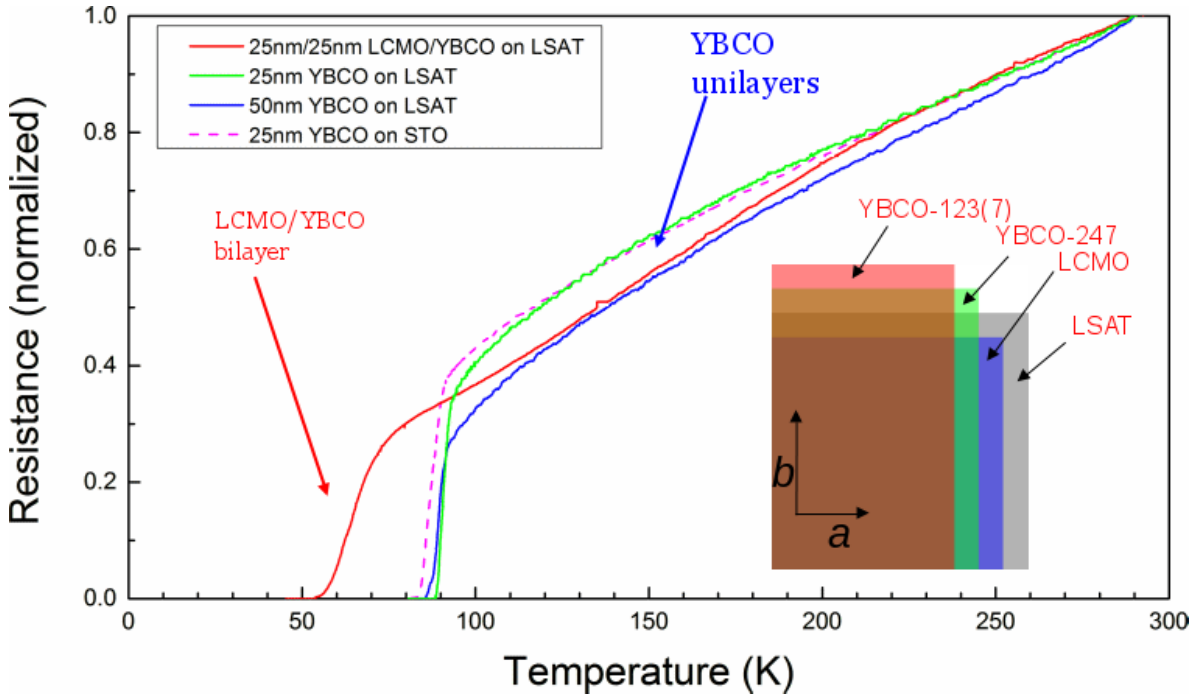

Figure 5: Plot of normalized resistance vs. temperature for unilayer YBCO and bilayer LCMO/YBCO films. All the unilayer films show sharp superconducting transitions with T_c near 90 K. The 25nm/25nm bilayer LCMO/YBCO film shows a broadened and reduced T_c near 60 K. The inset shows a schematic diagram illustrating the differences in both lattice symmetry and lattice parameters of the *ab*-plane lattice structure between YBCO-123, YBCO-247, LCMO, and LSAT. In the diagram, the relative length scales between the *a*- and *b*-axes for each material, and between the materials, are exaggerated for clarity.

To explain the formation of the nanoscale YBCO-247 regions in our LCMO/YBCO films and the absence of these intergrowths in unilayer YBCO films, we examine the lattice structures of the materials involved in the heteroepitaxy. It is well known that all the superconducting phases of Y-Ba-Cu-O are orthorhombic due to the CuO chain that runs along the *b*-axis. YBCO-

247 is less orthorhombic than YBCO-123, because of its shorter *b*-axis due to the inter-chain attraction within the double-CuO chains. As shown in the schematic diagram of the *ab*-plane lattice structures of YBCO-123, YBCO-247, LCMO, and LSAT in the inset of Figure 5, since both the LCMO overlayer and the LSAT substrate have cubic lattices, their combined mismatch in lattice symmetry with the YBCO layer would favor the formation of the less orthorhombic YBCO-247 phase. In addition to this lattice-symmetry mismatch, the *a*- and *b*-axes lattice parameters of both LCMO and LSAT are closer to YBCO-247 than to YBCO-123. Thus the lattice-parameter mismatch, from both sides of the YBCO layer, also tends to favor the formation of YBCO-247. In the YBCO layer, the conversion to YBCO-247 via the intergrowth of double CuO chains provides an effective mechanism for relieving the heteroepitaxial strain imposed by both the LCMO overlayer and LSAT substrate.

To examine the role played by magnetism in the T_c reduction of LCMO/YBCO heterostructures and to further corroborate our microstructural interpretation, we also grew LNO/YBCO heterostructures and measured their R vs. T for comparison. LNO is a paramagnetic perovskites with similar lattice parameters (within ~ 0.26%) as LCMO. Thus the YBCO layer in LNO/YBCO heterostructures is subject to similar heteroepitaxial strain as but without the ferromagnetism in LCMO/YBCO heterostructures. Figure 6 compares the R *vs* T plots for trilayer LNO/YBCO/LNO films with unilayer YBCO. All the samples were grown on (001)-oriented STO substrates. For the trilayer films, the YBCO layer was sandwiched between two LNO layers, each at 25 nm thick, to symmetrize the strain from both the top and the bottom

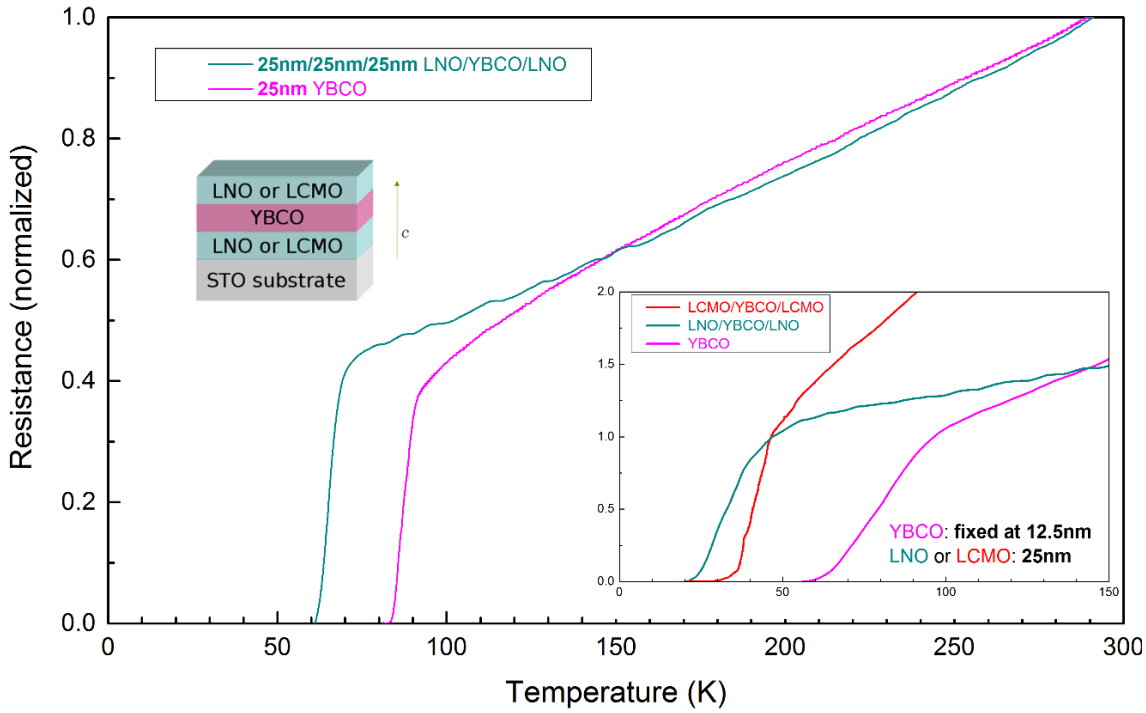

Figure 6: Plot of normalized resistance vs. temperature for trilayer LNO/YBCO/LNO and unilayer YBCO films grown on (001)-oriented STO substrates. In the trilayer, YBCO is sandwiched between two LNO layers each 25 nm thick. At 25 nm YBCO thickness, the trilayer film has a T_c ~ 60K, which is much lower than that of a unilayer YBCO film. The inset shows a comparison of the data between LNO/YBCO/LNO, LCMO/YBCO/LNO and unilayer YBCO, where the YBCO thickness is fixed at 12.5 nm. The onset of superconducting transition for LNO/YBCO/LNO occurs at the same temperature (~ 45K) as LCMO/YBCO/LCMO, and both have much lower T_c than unilayer YBCO.

sides. When the YBCO layer is at 25 nm, the trilayer film has a T_c near 60 K, which is much lower than that of a unilayer YBCO film but closer to that of LCMO/YBCO heterostructures when the YBCO layer is 25nm thick. A comparison of trilayer LNO/YBCO/LNO, trilayer LCMO/YBCO/LCMO and unilayer YBCO R vs. T with the YBCO layer fixed at 12.5 nm is shown in the inset. Here the trilayer films also have lower T_c than the unilayer film. In particular, the onset of the superconducting transition for the trilayer LNO/YBCO/LNO film occurs at almost the same temperature (~ 45K) as the trilayer LCMO/YBCO/LCMO film. Since LNO is not ferromagnetic, the similar dependence of T_c on YBCO layer thickness, between LNO/YBCO and LCMO/YBCO heterostructures, suggests that ferromagnetism plays a negligible role in the T_c reduction seen in the latter.

CONCLUSION

In summary, we have carried out a microscopic study of the superconducting proximity effect in LCMO/YBCO heterostructures. STS, STEM, XRD and electrical resistance measurements were performed on bilayer LCMO/YBCO and unilayer YBCO thin films, grown epitaxially on LSAT and STO substrates by PLD. For the STS measurement at 4.2K, bilayer LCMO/YBCO films down to 5nm LCMO thickness showed similar tunneling spectra as unilayer LCMO films, i.e. without proximity-induced pairing gaps. STEM images taken on the bilayer LCMO/YBCO films revealed YBCO-247 regions formed by double CuO-chain intergrowths, which can be attributed to heteroepitaxial lattice mismatch of the YBCO layer with both the LCMO overlayer and LSAT substrate. These nanoscale 247 regions do not appear in XRD, but can physically explain the lower resistive T_c measured in LCMO/YBCO multilayers. As further corroboration, we observed similar T_c reduction in LNO/YBCO multilayers, where LNO is not ferromagnetic. These results indicate that the anomalously long-ranged attenuation of superconductivity reported in LCMO/YBCO thin-film heterostructures are more likely due to microstructural defects than to magnetism.

ACKNOWLEDGEMENTS

Work supported by NSERC, CFI-OIT and the Canadian Institute for Advanced Research.

REFERENCES

[1] V. A. Vas'ko, V. A. Larkin, P. A. Kraus, K. R. Nikolaev, D. E. Grupp, C. A. Nordman, and A. M. Goldman, Phys. Rev. Lett. 78, 1134 (1997).
[2] P. Kraus, A. Bhattacharya, and A. M. Goldman, Phys. Rev. B 64, 220505(R) (2001).
[3] Z. Y. Chen, A. Biswas, I. Zutić, T. Wu, S. B. Ogale, R. L. Greene, and T. Venkatesan, Phys. Rev. B 63, 212508 (2001).
[4] Z. Sefrioui, D. Arias, V. Pena, J. E. Villegas, M. Varela, P. Prieto, C. Leon, J. L. Martinez, and J. Santamaria, Phys. Rev. B 67, 214511(2003).
[5] A. I. Buzdin, Rev. Mod. Phys. 77, 935 (2005).
[6] K. Dybko, K. Werner-Malento, P. Aleshkevych, M. Wojcik, M. Sawicki, and P. Przyslupski, Phys. Rev. B 80, 144504 (2009).
[7] For recent studies, see C. Visani, Z. Sefrioui, J. Tornos, C. Leon, J. Briatico, M. Bibes, A. Barthelemy, J. Santamaria, and J. E. Villegas, Nat. Phys. 8, 539 (2012), and references therein.
[8] H.-U. Habermeier, G. Cristiani, R. K. Kremer, O. Lebedev, and G. van Tendeloo, Physica C 364, 298 (2001).
[9] V. Pena, C. Visani, J. Garcia-Barriocanal, D. Arias, Z. Sefrioui, C. Leon, and J. Santamaria, Phys. Rev. B 73, 104513 (2006).

[10] F. S. Bergeret, A. F. Volkov, and K. B. Efetov, Phys. Rev. Lett. 86, 4096 (2001).
[11] F. S. Bergeret, A. F. Volkov, and K. B. Efetov, Rev. Mod. Phys. 77, 1321 (2005).
[12] R. S. Keizer, S. T. B. Goennenwein, T. M. Klapwijk, G. Miao, G. Xiao and A. Gupta, Nature 439, 825 (2006).
[13] Y. Asano, Y. Tanaka, A. A. Golubov, and S. Kashiwaya, Phys. Rev. Lett. 99, 067005 (2007).
[14] Z. Ping Niu and D. Y. Xing, Phys. Rev. Lett. 98, 057005 (2007).
[15] Y. Kalcheim, T. Kirzhner, G. Koren, and O. Millo, Phys. Rev. B 83, 064510 (2011).
[16] Roland Grein, Tomas Löfwander, and Matthias Eschrig, Phys. Rev. B 88, 054502 (2013).
[17] V. I. Zdravkov, J. Kehrle, G. Obermeier, D. Lenk, H.-A. Krug von Nidda, C. Müller, M. Yu. Kupriyanov, A. S. Sidorenko, S. Horn, R. Tidecks, and L. R. Tagirov Phys. Rev. B 87, 144507 (2013).
[18] T. Golod, A. Rydh, V. M. Krasnov, I. Marozau, M. A. Uribe-Laverde, D. K. Satapathy, Th. Wagner, and C. Bernhard, Phys. Rev. B 87, 134520 (2013).
[19] M. Egilmez, J. W. A. Robinson, Judith L. MacManus-Driscoll, L. Chen, H. Wang and M. G. Blamire, Europhys. Lett. 106, 37003 (2014).
[20] A. Singh, S. Voltan, K. Lahabi, and J. Aarts, Phys. Rev. X 5, 021019 (2015).
[21] C. C. Tsuei and J. R. Kirtley, Rev. Mod. Phys. 72, 969 (2000).
[22] J. Y. T. Wei, N.-C. Yeh, D. F. Garrigus, and M. Strasik, J. Y. T. Wei, N.-C. Yeh, D. F. Garrigus, and M. Strasik (1998).
[23] T. Holden, H.-U. Habermeier, G. Cristiani, A. Golnik, A. Boris, A. Pimenov, J. Humlicek, O. I. Lebedev, G. Van Tendeloo, B. Keimer, and C. Bernhard, Phys. Rev. B 69, 064505 (2004).
[24] M. Varela, A. R. Lupini, V. Pena, Z. Sefrioui, I. Arslan, N. D. Browning, J. Santamaria, and S. J. Pennycook, e-print arXiv:cond-mat/0508564 (2006).
[25] V. Pena, T. Gredig, J. Santamaria, and I. K. Schuller, Phys. Rev. Lett. 97, 177005 (2006).
[26] J. Chakhalian, J. W. Freeland, H.-U. Habermeier, G. Cristiani, G. Khaliullin, M. van Veenendaal, and B. Keimer, Science 318, 1114 (2007).
[27] J. Chakhalian, J. W. Freeland, G. Srajer, J. Strempfer, G. Khaliullin, J. C. Cezar, T. Charlton, R. Dalgliesh, C. Bernhard, G. Cristiani, H.-U. Habermeier, and B. Keimer, Nat. Phys. 2, 244 (2006).
[28] J. Stahn, J. Chakhalian, C. Niedermayer, J. Hoppler, T. Gutberlet, J. Voigt, F. Treubel, H.-U. Habermeier, G. Cristiani, B. Keimer, and C. Bernhard, Phys. Rev. B 71, 140509(R) (2005).
[29] L. Crétinon, A. K. Gupta, H. Sellier, F. Lefloch, M. Faure, A. Buzdin, and H. Courtois, Phys. Rev. B 72, 024511 (2005).
[30] I. Asulin, O. Yuli, G. Koren, and O. Millo, Phys. Rev. B 74, 092501 (2006).
[31] I. Asulin, O. Yuli, I. Felner, G. Koren, and O. Millo, Phys. Rev. B 76, 064507 (2007).
[32] P. C. van Son, H. van Kempen, and P. Wyder, Phys. Rev. Lett. 59, 2226 (1987).
[33] R. J. Cava, B. Batlogg, R. B. van Dover, D. W. Murphy, S. Sunshine, T. Siegrist, J. P. Remeika, E. A. Rietman, S. Zahurak, and G. P. Espinosa Phys. Rev. Lett. 58, 1676 (1987).
[34] P. Bordet, C. Chaillout, J. Chenavas, J. L. Hodeau, M. Marezio, J. Karpinski, and E. Kaldis, Nature 334, 596 (1988).
[35] D. E. Morris, J. H. Nickel, J. Y. T. Wei, N. G. Asmar, J. S. Scott, U. M. Scheven, C. T. Hultgren, A. G. Markelz, J. E. Post, P. J. Heaney, D. R. Veblen, and R. M. Hazen, Phys. Rev. B 39, 7347 (1989).
[36] D. E. Morris, N. G. Asmar, J. Y. T. Wei, J. H. Nickel, R. L. Sid, J. S. Scott, and J. E. Post, Phys. Rev. B 40, 11406 (1989).
[37] J. Karpinski, E. Kaldis, S. Rusiecki, E. Jilek, P. Fischer, P. Bordet, C. Chaillout, J. Chenavas, J. L. Hodeau, and M. Marezio, Physica C 160, 449 (1989).
[38] J. Karpinski, S. Rusiecki, B. Bucher, E. Kaldis, and E. Jilek, Physica C 161, 618 (1989).

[39] J. L. Tallon, D. M. Pooke, R. G. Buckley, M. R. Presland, and F. J. Blunt, Phys. Rev. B 41, 7220 (1990).
[40] H. Zhang, N. Gauquelin, G. A. Botton, and J. Y. T. Wei, Appl. Phys. Lett. 103, 052606 (2013).
[41] I. Fridman, L. Gunawan, G. A. Botton, and J. Y. T. Wei, Phys. Rev. B 84, 104522 (2011).
[42] N. Gauquelin, G.-z. Zhu, H. Zhang, J. Y. T. Wei and G. A. Botton, submitted to Adv. Mater. Commun. (2015).
[43] A. K. Raychaudhuri, K. P. Rajeev, H. Srikanth, and N. Gayathri, Phys. Rev. B 51, 7421 (1995).
[44] J. J. Capponi, C. Chaillout, A. W. Hewat, P. Lejay, M. Marezio, N. Nguyen, B. Raveau, J. L. Soubeyroux, J. L. Tholence, and R. Tournier, Europhys. Lett. 3, 1301 (1987).
[45] M. Kato, M. Nakanishi, T. Miyano, T. Shimizu, M. Kakihana, K. Yoshimura, and K. Kosuge, J. Solid State Chem. 139, 266 (1998).
[46] A. Irizawa, T. Ohmura, T. Shibata, M. Kato, K. Yoshimura, K. Kosuge, Y. Ito, H. Michor, and G. Hilscher, J. Phys. Soc. Jpn. 71, 574 (2002).